Research Square

Preprints are preliminary reports that have not undergone peer review.
They should not be considered conclusive, used to inform clinical practice,
or referenced by the media as validated information.

APOE4 Alters the Inflammatory and Metabolic Properties of Extracellular Vesicles of Induced Pluripotent Stem Cell-derived Astrocytes and Mesenchymal Stromal Cells

Colin Esmonde
Florida State University
Ana-Caroline Raulin
Mayo Clinic in Florida
Tammee Parsons
Mayo Clinic in Florida
Jennifer Berg Sen
Florida State University
Yeoheung Yun
North Carolina Agricultural and Technical State University
Takahisa Kanekiyo
Mayo Clinic in Florida
Yan Li
yli4@fsu.edu

Florida State University

Research Article

Keywords: Human pluripotent stem cells, extracellular vesicles, APOE4, astrocytes, mesenchymal stem cells, lipidomics

Posted Date: November 13th, 2026

DOI: https://doi.org/10.21203/rs.3.rs-11104163/v1

License: This work is licensed under a Creative Commons Attribution 4.0 International License.
Read Full License

Additional Declarations: No competing interests reported.

APOE4 Alters the Inflammatory and Metabolic Properties of Extracellular Vesicles of Induced Pluripotent Stem Cell-derived Astrocytes and Mesenchymal Stromal Cells

Colin Esmonde[1], Ana-Caroline Raulin[2], Tammee Parsons[2], Jennifer Berg Sen[1], Yeoheung Yun[3], Takahisa Kanekiyo[2, *], Yan Li[1, 2, *]

[1]Department of Chemical and Biomedical Engineering, FAMU-FSU College of Engineering, Florida State University, Tallahassee, FL, USA

[2]Mayo Clinic, Jacksonville, FL, USA

[3]Department of Chemical, Biological, and Bioengineering, North Carolina Agricultural and Technical State University, Greensboro, NC 27411, USA

***Corresponding authors:**

Dr. Yan Li: address: 2525 Pottsdamer St., Tallahassee, FL 32310, USA, Tel: 850-410-6320; Fax: 850-410-6150; email: yli4@fsu.edu. ORCID: Yan Li: 0000-0002-5938-8519

Dr. Takahisa Kanekiyo, email: kanekiyo.takahisa@mayo.edu

Contact information for other authors:

Colin Esmonde: email: cme18b@fsu.edu

Dr. Ana-Caroline Raulin: email: raulin.ana-caroline@mayo.edu

Dr. Tammee Parsons: email: parsons.tammee@mayo.edu

Jennifer Berg Sen: email: jlb21a@fsu.edu

Dr. Yeoheung Yun: email: yyun@ncat.edu

Submitted to *Stem Cell Research & Therapy*

Abstract:

Background: Apolipoprotein E (APOE) is a lipid transporter whose variant, *APOE4*, is the strongest genetic predictor of Alzheimer's disease development. APOE's role as a lipid transporter is disrupted with E4 due to differences in its binding affinity, altering APOE's preferred lipid substrate. This alters the cholesterol homeostasis of neural cells such as astrocytes, leading to lipid droplet formation, a driver of neuroinflammation. In addition, APOE has been identified as a cargo protein carried within extracellular vesicles (EVs), including exosomes, suggesting EVs play a role in regulating neural lipid metabolism. However, the extent and further results of APOE disruption of EV excretion and cargo are not well-established.

Methods: This study seeks to identify differences in EV secretion and bioactivity between *APOE3* and *APOE4* genotypes in various cell types and the role they play in Alzheimer's disease pathogenesis. Human pluripotent potent stem cell-derived astrocytes (iASs) and mesenchymal stromal cells (iMSCs) with homozygous *APOE3* and homozygous *APOE44* cellswere derived and the secreted EVs were characterized.

Results: Our results indicate that EV secretion was comparable in *APOE3* and *APOE4* cells, although decreased expression of the endosomal sorting complex required for transport (ESCRT) dependent and independent genes in *APOE4* cells was observed. When treating THP-1 cells, an innate inflammatory capability is observed across cell types in APOE4 EVs, increasing the levels of NF-κB activation significantly compared to untreated controls. Quantitative lipidomics revealed increased levels of total lipid and lipid classes involved in the mediation of lipid stress in APOE4 EVs. In addition, lipids involved in EV biogenesis are dysregulated. KEGG analysis showed upregulation of functional pathways of interest in Alzheimer's Disease progression, including efferocytosis, choline metabolism, and bile acid synthesis.

Conclusions: Our results suggest that APOE4 may affect the lipid cargo of the EVs, which is hypothesized to be a result of endosomal trafficking via interruptions in both ESCRT dependent and independent biogenesis pathways. Furthermore, disrupted lipid metabolism in APOE4 could affect ESCRT-independent EV formation. APOE4 derived EVs have innate inflammatory properties that are exacerbated in the presence of excess fatty acid. This study paves the way for understanding the role of EVs in mediating inflammation and lipid metabolism in APOE4 related Alzheimer's disease.

Key words: Human pluripotent stem cells, extracellular vesicles, APOE4, astrocytes, mesenchymal stem cells, lipidomics

1. Introduction

Alzheimer's disease (AD) is a leading cause of dementia, leading to 60-80% of all cases in the United States [1]. While AD has been extensively studied, its origins have not been clearly determined, though several theories have been put forth and risk factors identified. Among known risk factors, the strongest predictor of AD development is the *E4* variant of apolipoprotein E. Apolipoprotein E, or APOE, is an extracellular lipid transporter that is mainly synthesized in the liver and the brain. Normally, APOE binds and transports cholesterol and phospholipids throughout the body by binding with lipoprotein particles, binding high-density, low-density, and very low-density lipoproteins (e.g., HDLs, LDLs, and vLDLs, respectively) [2, 3]. After its incorporation, it facilitates the cellular uptake of lipoprotein particles via interaction with cell receptors such as LRP and LDLR [4]. In neural tissue, it helps regulate neuronal metabolism, transporting cholesterol and lipids from astrocytes to neurons [5]. However, its central role as a metabolic regulator in neural tissue means that *APOE* variants can differentially and significantly affect the central nervous system (CNS).

APOE has three isoforms: APOEAPOE2, APOE3, and APOE4. Of those, APOE3 is the most commonly occurring one, accounting for 75% of APOE alleles, while APOE2 is the least common [6]. The single amino-acid substitution seen in APOE4 alters salt bridge formation within the protein, ultimately leading to an altered lipid binding domain. This change alters the lipoprotein binding preference of APOE from HDLs in unmutated APOE to vLDLs [7, 8]. HDLs act as scavengers, associating with excess cholesterol and facilitating its cellular uptake [9, 10]. In neural tissue, the loss of HDL binding affinity seen in APOE4 translates to a disruption in cholesterol scavenging and transport, leading to lipid accumulation in microglia, astrocytes, and neurons [11, 12] .

In AD pathology, the altered lipid binding site of APOE4 has several implications. The disruption of APOE4’s lipid binding leads to the accumulation of excess lipid in astrocytes and microglia, contributing to lipid droplet formation and consequentially inflammation due to lipid stress, linking to neuroinflammation [13, 14]. Along with acting as a lipid transporter, APOE particles can mediate the clearance of peptides such as amyloid β. However, APOE4 does not bind well to soluble amyloid peptides, contributing to the surplus amyloid β commonly associated with AD development. The altered binding site also interacts with insoluble amyloid β, serving as a seeding site for the development of amyloid plaques [15-17]. Other mechanisms, such as the mechanisms of lipid exchange between astrocytes and neurons, are only partially understood. APOE lipoprotein particles help regulate the transport of lipids from astrocytes to neurons [18-20].

The APOE4 isoform's preference of vLDLs is associated with changes in lipoprotein particle composition, size, and function in regulating neuron metabolism [21, 22]. In addition, APOE4 exhibits lower binding affinity with the lipoprotein receptor LRP1, which further inhibits the clearance of APOE4 particles and amyloid β, a peptide fragment that aids in AD progression [23].

Recently, APOE has been shown to be associated with extracellular vesicles (EVs), in particular the small size EV subpopulation exosomes (30-200 nm), to facilitate lipid transport [24, 25]. Exosomes have specific lipids packed into their membrane to participate in selective lipid transport, further complicating their role in lipid metabolism [26, 27]. Exosomes also serve as a method of intracellular communication, carrying proteins and miRNAs between cells. Within AD, exosomes can aid disease progression by trafficking toxic proteins between cells and by serving as a seeding spot for amyloid plaques [28, 29]. Given the differential role that APOE isoformscan play in mediating amyloid trafficking and seeding, it is possible that APOE displayed in exosomes aids in EV-mediated disease progression.

To fully understand the role of APOE4 in AD progression and identify effective novel therapeutics, this study seeks to understand the role that APOE genotype has on EV biogenesis, inflammatory properties, and the lipid content of EVs derived from different APOE cell types, based on human induced pluripotent stem cell (iPSC) technology. Astrocytes (iAS) and mesenchymal stromal cells (iMSCs) were derived from iPSCs with isogenic APOE3 and APOE4 genetic background. The secreted EVs were isolated and characterized for yield, size, morphology and marker expression. The abilities of the EVs with different genetic backgrounds in inflammatory modulation and the effects of lipid stress on EV secretion and functional properties were also investigated. In particular, quantitative lipidiomics was performed to reveal the lipid composition of the EVs with different genetic backgrounds, where the increased lipid contents including cholesterol, biliary acids, sphingolipids, and lysophospholipids etc.in EVs of APOE4 group were observed compared to APOE3 group. This study reveals the potential of healthy EVs in correcting lipid metabolism and the importance of lipid modulators in preventing neural degeneration.

2. Materials and Methods

2.1. Human iPSC culture

Human iPSCs from the KOLF2 and APOE C112R SNV/SNVcell lines were obtained from the Jackson Laboratory (Bar Harbor, Maine). iPSCs were thawed and plated onto growth factor reduced Matrigel (Life Technologies)-coated 6 well plates in mTeSR Plus (StemCell Technologies, Inc., Vancouver, Canada) supplemented with 10 μM rho-associated protein kinase (ROCK)

inhibitor Y27632 (Sigma). After 1 day, cells were switched to mTeSR Plus and subject to daily medium changes. After 5-7 days, cells were passaged using Accutase (StemCell Technologies).

2.2. Astrocyte differentiation from iPSCs (iASs)

To induce neural progenitor differentiation, iPSCs were seeded into 96 well plates in STEMdiff Neural Induction Media (StemCell Technologies) supplemented with SMAD inhibitors 10 μM SB431542 (Sigma) and 100 nM LDN193189 (Sigma) along with 10 μM ROCK inhibitor Y-27632 for 5 days to generate embryoid bodies. On day 5, embryoid bodies were replated for another 6-7 days of culture. On day 11-12, neural rosettes were selected and replated for 6-7 days. On day 17-19, neural progenitor cells were dissociated into a single-cell suspension before replating in STEMdiff Neural Progenitor Medium (StemCell Technologies) for 7 days, after which cells were considered mature neural progenitor cells. For astrocytic differentiation, neural progenitor cells were replated in ScienCell Astrocyte Medium (ScienCell Research Laboratories, Carlsbad, CA) and cultured for 21 days, being passaged every 6-7 days as needed. After day 21, cells were considered mature astrocytes and subcultured in ScienCell Astrocyte Medium (ScienCell Research Laboratories).

2.3. MSC differentiation from iPSCs (iMSCs)

To induce mesenchymal stromal cell differentiation, a single-cell suspension of 15,000 iPSCs were seeded into U bottom 96 well plates suspended in Induction Medium composed of IMDM supplemented with 20% KnockOut Serum, 0.1 mM nonessential amino acids (Gibco, Billings, Mt), 0.1 mM 2-mercaptoethanol, and 10 μM Y-27632 on day 0. On day 2, 4-5 embryoid bodies were seeded onto non-tissue treated 6 well plates in media prepared as before. After 3 days, on day 5, embryoid bodies were seeded onto 6 well plates coated with 1% gelatin in Induction Medium for 3 days. On day 8, Induction Medium was replaced with Differentiation medium composed of IMDM, 20% KnockOut Serum, 0.1 mM nonessential amino acids (Gibco, Billings, Mt), 0.1 mM 2- mercaptoethanol, and 100 μg/mL TGFB1 for 3 days. From day 11 onwards, differentiation media was replaced with αMEM supplemented with 5% fetal bovine serum and 1% Glutamax (Gibco, Billings, Mt).

2.4. Flow cytometry

APOE33 and *APOE44* iMSC were cultured under standard conditions and analyzed at passage 3 (P3). Cells were harvested at approximately 70–80% confluency using TrypLE Express Enzyme (Gibco, A1217701) and resuspended in flow cytometry staining buffer consisting of Dulbecco's Phosphate Buffered Saline (DPBS) supplemented with 1–2% bovine serum albumin and Sodium Azide. Approximately 1×10^5 cells per sample were incubated with the antibody panel

for 30 minutes at room temperature in the dark. Following incubation, cells were washed with staining buffer and resuspended for flow cytometric analysis. Positive MSC markers included CD90, CD73, and CD105, detected using the following antibodies: BD Stemflow FITC-conjugated anti-human CD90 (BD Biosciences,51-9007657), BD Stemflow APC-conjugated anti-human CD73 (BD Biosciences, 51-9007649), and PE-Vio® 770–conjugated anti-human CD105 (Miltenyi Biotec,130-099-890) (**Supplementary Table S1**). Negative marker expression was assessed using a BD Stemflow PE hMSC Negative Cocktail (BD Biosciences, 51-9007661), containing antibodies against CD34, CD45, CD11b, CD19, and HLA-DR. Unstained and isotype control samples were included to establish background fluorescence and define gating parameters. Data was acquired using an Invitrogen Attune NxT Flow Cytometer (Thermo Fisher Scientific) analyzed by gating strategy to exclude debris, identify single cell population and confirm surface marker expression.

2.5. Enzyme-linked immunosorbent assay (ELISA) for APOE secretion

APOE33 and *APOE44* iAS were plated at the same density and conditioned the next day in serum-free astrocyte medium for 3 days. APOE medium was collected at different time points throughout differentiation (at days 10, 20, 30 and 40). APOE in medium was quantified by sandwich ELISA [30]. Briefly, an ELISA 96-well plate was coated with a monoclonal antibody directed against APOE (WUE-4, Novus) as a capture antibody in Coating Buffer (0.05M Carbonate buffer pH 9.6) overnight at 4ºC. Plates were blocked in Blocking Buffer (1% (w/v) Block Ace (Bio-Rad BUF029) in PBS, 0.05% NaN_3) for an hour at room temperature. Samples were added to the plate in Diluent Buffer (25 mM phosphate, pH 7.0 containing 0.4 M NaCl, 2.5 mM EDTA, 0.2% BSA, 0.4% Block Ace, 0.05% CHAPS, and 0.05% NaN_3) and incubated overnight at 4ºC. A biotin-conjugated polyclonal anti-APOE antibody in Diluent Buffer (K74180B, Meridian Life Sciences) was used as detection antibody. An HRP-streptavidin conjugate antibody diluted in HRP Dilution Buffer (25 mM phosphate, pH 7.0 supplemented with 0.4 M NaCl, 2 mM EDTA, 1% (w/v) BSA, and 0.002% (w/v) thimerosal) was used to bind the biotinylated detection antibody. Sandwich ELISAs were developed following addition of 3,3′,5,5′- tetramethylbenzidine (TMB) substrate. The reaction was halted with 1M sulfuric acid. Absorbance was measured at 450 nm using a Synergy HT microplate reader (BioTek). Target protein levels were determined using a standard curve generated with recombinant APOE.

2.6. Immunostaining

iAS were plated at 12,500 cells/cm^2 for immunostaining purposes. The following day, cells were fixed for 10 min with 4% PFA, permeabilized with 0.3% Triton-X 100 in PBS for 10 min, and

blocked in Blocking Buffer (1% BSA in PBS, Milteny Biotec, 130-091-376) for 1 hour. Cells were incubated with an anti-GFAP (PA5-18598, Thermo Fisher) and an anti-S100β (S2532, Sigma Aldrich) antibody in Blocking Buffer overnight at 4ºC, followed by fluorescently labelled secondary antibodies (anti-goat, IgG H+L Alexa Fluor™ 488, A11055 and anti-mouse, IgG H+L Alexa Fluor™ 568, A10037, Invitrogen) for 1 hour at room temperature. DAPI was used as nuclear counterstain. Images were obtained on a Keyence BX100 microscope.

2.7. EV isolation based on differential ultracentrifugation

To isolate EVs, a differential ultracentrifugation protocol was employed as seen in our previous publications [31-34]. Three days before media collection, cells were switched to a cell culture medium containing EV-depleted fetal bovine serum (FBS). Spent culture medium was centrifuged at 500 g for 5 minutes before discarding the pellet. Supernatant was then centrifuged at 2000 g for 10 minutes and the resulting pellet discarded, and the resulting supernatant was centrifuged at 10,000 g for 30 minutes at 4°C before again discarding the pellet. A half-volume of a solution containing 16% polyethylene glycol (PEG) and 1.5 M NaCl was added to supernatant, mixed via inversion, and allowed to sit overnight at 4°C. On the next day, media was centrifuged at 3000 g for 1 hour at 4°C before discarding the supernatant. The resulting pellets were resuspended in 1 mL of milli-Q PBS. Resuspended pellets were ultracentrifuged at 127,000 g for 70 minutes at 4°C. The supernatant was then discarded and the pellets resuspended in 200 µL milli-Q PBS and shaken for 15 minutes. The freshly isolated exosomes were stored at either 4°C or -80°C before further analysis.

2.8. Nanoparticle Tracking Analysis (NTA)

NTA was performed to characterize isolated EV size and concentration using a NanoSight Nano Sight NS300. Exosomes were diluted 1:1000 in milli-Q PBS before NTA. 5 videos of 30 second duration were taken, with the camera level set to 11 and the detection threshold set at default. Between each reading, fresh sample was added to the view field by depressing the syringe containing sample. Between samples, the NTA chamber was washed with Contrad 70 (Decon Labs, Inc), then milli-Q water, before the next sample was read. Resulting videos were analyzed using NTA 3.4 software to give mean and mode particle size, as well as particle concentration.

2.9. Transmission Electron Microscopy (TEM)

TEM was used to characterize the shape of isolated exosomes. To do so, a 15 µL drop of exosome suspension was placed onto parafilm sheet and a carbon-coated 400 Hex Mesh Copper Grid (Electron Microscopy Sciences, EMS) placed face-down on the drop for 60 minutes.

Afterwards, the grids were washed 3 times in milli-Q PBS by transfer onto 30 µL drops. Grids were dried between washes with absorbing paper by gently tapping the side of grids, avoiding contact with the coating side. Next, grids were placed on a 20 µL drop of 2% paraformaldehyde for 10 minutes. Grids were washed again in PBS. After drying, grids were stained by placement on a 20 µL drop of 2% uranyl acetate before being embedded on a drop of 0.13% Methyl cellulose and 0.4% uranyl acetate for 10 minutes. Afterwards, grids were dried using absorbing paper and left to dry overnight coated-side up overnight.

2.10. Reverse Transcription quantitative Polymerase Chain Reaction (RT-qPCR)

To isolate mRNA for PCR analysis, approximately 1 million cells per sample were lysed using the Qiagen RNEasy Plus kit (Qiagen, Hilden, Germany) was used according to vendor instructions. Isolated RNA was cleaned in column using the RNA Clean and Concentrator kit (Zymo Research, California, USA) according to manufacturer's instructions. Reverse transcription was carried out using 2 µg of total RNA, anchored oligo-dT primers (Operon) and Superscript III (Invitrogen). Primers were designed using the software Oligo Explorer 1.2 (Genelink) (**Supplementary Table S2**). RT-PCR reactions were performed on an ABI7500 instrument (Applied Biosystems), using a SYBR Green PCR Master Mix. Fold variations in gene expressions were quantified using the delta-delta Ct approach: $2^{-(\Delta C_{t\ treatment} - \Delta C_{t\ Control})}$, which is based on the comparison of the target gene (normalized to GAPDH) among different conditions.

2.11. Western blot for exosomal markers

EV and cell samples were lysed in radio-immunoprecipitation assay (RIPA) buffer (150 mM sodium chloride, 1.0% Triton X-100, 0.5% sodium deoxycholate, 0.1% sodium dodecyl sulphate, 50 mM Tris, pH8 and 1X Thermo Scientific™ Halt™ Protease Inhibitor Cocktail) (Thermo Fisher Scientific Inc., Waltham, MA, USA). Samples were incubated for 20 min on ice, and spun down at 14,000 rpm for 20 min. The cleared supernatants were collected, and a Bradford assay was carried out to determine protein concentration. Protein lysate concentration was normalized, and denatured at 100°C in 2 × Laemmli Sample buffer for 5 min. About 3–10 µg of proteins were loaded into each well. Proteins were separated by 12% Bis-Tris-SDS gels and transferred onto a nitrocellulose membrane (Bio-Rad, Hercules, CA. USA). For the detection of non-phosphorylated proteins, the membranes were blocked for 1 hour in 1% (w/v) non-fat dry milk in Tris-buffered saline (10 mM Tris-HCl, pH 7.5 and 150 mM NaCl) with 0.1% (v/v) Tween 20 (TBST). After transfer, membranes were stained with Ponceau solution for 5 minutes and imaged before being cut based upon molecular weight markers (**Supplementary Figure S1**). Membranes were incubated overnight in the presence of the primary antibodies (**Supplementary Table S1**)

diluted in Blocking Buffer at 4°C. Afterwards, the membranes were washed four times with TBST and then incubated with a horseradish peroxidase (HRP)-conjugated secondary antibody at 1:5000 for 1 hour. The blots were washed and imaged on the Biorad ChemiDoc Imaging System.

2.12. Lipidomics analysis of EV lipid composition

Quantitative Lipidomics was performed by Metware Biotechnology Inc. The samples were taken out from the -80°C refrigerator and thawed on ice. 1 mL of the extraction solvent (MTBE: MeOH =3:1, v/v) containing internal standard mixture was added to the samples. After whirling the mixture for 15 min, 200 µL of ultrapure water was added. The samples were vortexed for 1 min and centrifuged at 12,000 rpm for 10 min. 500 µL of the upper organic layer was collected and evaporated using a vacuum concentrator. The dry extract was dissolved in 200 µL reconstituted solution (ACN: IPA=1:1, v/v) prior to liquid chromatography-tandem mass spectrometry (LC-MS/MS) analysis. The data acquisition instruments consisted of Ultra Performance Liquid Chromatography (UPLC) (Nexera LC-40) and tandem mass spectrometry (MS/MS) (Triple Quad 6500). With in-house database, lipids were annotated based on their retention time and ion-pair information from Multiple Reaction Monitoring (MRM) mode. In MRM mode, the first quadrupole screens the precursor ions for target substance and excluded ions of other molecular weights. After ionization induced by the impact chamber, the precursor ions were fragmented, and a characteristic fragment ion was selected through the third quadrupole to exclude the interference of other non-target ions.

2.13. Immunomodulation assay

To test the role *APOE* variants play on exosome-mediated inflammation, an immunomodulation assay was performed using a NF-κB- luciferase reporter THP-1 line (ATCC) in a live cell luciferase reporter assay. 1 million THP-1 cells were seeded into 6 well plates in RPMI media supplemented with 10% FBS. For lipopolysaccharide (LPS) positive groups, cells were treated with 100 ng/mL LPS for 6 hours before receiving fresh media. All samples receiving exosomes had their respective doses added before being allowed to incubate overnight at 37°C. Afterwards, cell suspensions were collected and aliquoted into a 96 well plate at 100 µL per well and the luminescence was measured using the One-Glo luciferase assay system (Promega, E6120) according to the manufacturer's protocol.

2.14. Oleic acid-based assay

To test the role of exosome mediation of lipid stress, a lipid stress model was employed using oleic acid. Either oleic acid (Sigma) dissolved in DMSO (Sigma) or an equal volume of DMSO vehicle was added to parent cells at 50 µM in EV depleted culture medium and allowed to

incubate for 72 hours, after which spent media was collected for EV isolation. Isolated EVs were then used to treat THP-1 cells in an immunomodulation assay as previously described.

2.15. Statistical analysis

All experiments were performed in biological triplicate (n=3), and representative data were reported. Experimental results were expressed as means ± standard deviation (SD). Statistical comparisons were performed by one-way ANOVA and Tukey's post hoc test for multiple comparisons, and significance was accepted at $p < 0.05$ using GraphPad Prism. For comparisons of two conditions, student's t-test was performed for the statistical analysis.

3. Results

3.1. Characterization of iASs and iMSCs.

APOE33 and *APOE44* iPSC-to-astrocytes differentiation was achieved via neural progenitor cells (**Figure 1A**). iPSC-derived astrocytes (iAS) identity was verified through the expression of astrocyte-specific markers GFAP and S100β by immunostaining at day 30+ (**Figure 1B**). Both *APOE33* and *APOE44* iAS express APOE, which can be detected in media as APOE is a secreted protein. While levels of APOE in media vary with differentiation stages, they are overall detected at higher levels in APOE33 iAS **(Figure 1C**). *APOE33* and *APOE44* iPSC-to-MSC conversion occurred over approximately 2 weeks using induction medium supplemented with TGFβ1 (**Figure 2A**). *APOE33* and *APOE44* iPSC-derived MSC (iMSC) were confirmed to express over 95% for the cell surface markers CD105 and CD73 and CD90 and less than 5% CD34, CD45, CD11b, CD19, or HLA-DR when analyzed at passage 3 (**Figure 2B and 2C, Supplementary Figure S2**).

3.2. Characterization of EVs secreted from Cells of Different APOE Genotypes

To begin experimentation, exosomes were isolated from iAS and mesenchymal stromal cells (iMSCs) from iPSCs that were isogenic save a point mutation that changed the genotype of one from APOE3/E3 to APOE4/E4. The pellets received after isolation were characterized using NTA. Astrocyte-derived exosomes from both genotypes displayed a characteristic size profile, with mean and median diameters falling below 200 nm (**Figure 3A, 3B**). To analyze exosome yield, overall yield was normalized to cell count and media expenditure for each culture. When normalized to cell number, a significant decrease in exosome production is seen in the *APOE4* iAS group when compared to its *APOE3* counterpart (**Figure 3C**). When normalized by media expenditure, no difference is observed between iAS groups (**Figure 3D**). Transmission electron

microscopy images of isolated iAS EVs for both *APOE3* and *APOE4* groups revealed typical cup shape morphology indicative of exosomal identity (**Figure 3E**). Western blot analysis showed that the EVs were positive for exosomal markers CD81 and TSG101 (**Figure 3F**). The EVs also showed no expression on negative exosomal marker Calnexin which was positive in cells.

The endosomal sorting complex required for transport (ESCRT) gene expression was investigated to account for the differences seen in exosome per cell yield between astrocytes from different genotypes. The results show significant decreases in the expression of ESCRT dependent exosome biogenesis genes ALIX, STAM1, and STAM2 in *APOE4* astrocytes. Similarly, *APOE4* astrocytes expressed significantly lower levels of ESCRT independent exosome biogenesis genes RAB27a, SMPD2, and SMPD3 (**Figure 3G**). Overall, this suggests that exosome biogenesis is disrupted in *APOE4* astrocytes through both ESCRT dependent and independent pathways.

Similarly, iMSC-derived EVs displayed mean and median sizes within the typical morphology of exosomes, though with a larger deviation (**Figure 4A,4B**). Normalization of exosome yield to cell number per day of collection and to spent media volume revealed no significant differences between *APOE* genotypes (**Figure 4C,4D**). Overall, these results suggest that differences in *APOE* genotype can affect exosome secretion depending on the cell type exosomes are secreted from. TEM images of isolated iMSC EVs for both APOE3 and APOE4 groups revealed typical cup shape morphology for exosomes (**Figure 4E**). Western blot analysis showed that the EVs were positive for exosomal markers HSC70, CD81, and TSG101 (**Figure 4F**). The EVs also showed no expression on negative exosomal marker Calnexin.

3.3. APOE Genotype Dictates the Inflammatory Characteristics of EVs

To evaluate the potential role of exosomes in the development and progression of APOE4-related AD, an inflammatory activation assay was employed, using luciferase NF-κB reporter THP-1 cells. Initially, only exosomes were added to THP-1 cultures, with a single experimental group receiving LPS activation for 6 hours before receiving a media change (not graphed to enhance clarity). This was done to determine any effects *APOE* genotype may have on innate exosome inflammatory properties, as neuroinflammation is a hallmark symptom of AD. Luciferase assays using iAS exosomes revealed that at lower doses (1E8 exosomes/mL THP-1 media), no significant differences between experimental groups were observed (**Figure 5A**). At high doses (1E9 exosomes/mL THP-1 media), a significant increase in NF-κB activity was observed in exosomes from the *APOE4* genotype. This was not recorded in APOE3 exosomes (**Figure 5B**). Similarly, exosomes from iAS cells with different *APOE* genotypes were added to THP-1 cells that

were pretreated with LPS for 6 hours to assess their ability to inhibit inflammation. At low doses, EVs from *APOE3* cells inhibited inflammation, an aspect that is not shared by exosomes from *APOE4* iAS cells (**Figure 5C**). However, at higher doses, no differences were observed between LPS groups (**Figure 5D**).

A similar set of experiments was performed for exosomes derived from iMSCs. In this set of experiments, an increase in THP-1 NF-κB activity was observed at low doses for cells treated with APOE4 exosomes (**Figure 5E**). For iMSC exosomes at low doses, no differences were observed between LPS groups (**Figure 5F**). Data for high dosage iMSCs is still in progress. These results further support the theory that differences in *APOE* genotype confer differences in inflammatory regulation. Overall, these results suggest that exosomes from *APOE4* cells have different inflammatory properties compared to their *APOE3* counterparts. The cause of this remains unknown, however.

3.4. APOE Genotype Alters Exosome Secretion and Signaling Under Lipid Stress

One of the symptoms present in AD that results from APOE4 is stress caused by excess lipid buildup in neural tissue. To investigate how this affects exosome secretion and signaling under lipid stress, oleic acid, a fatty acid that contributes to lipid stress in Alzheimer's progression, was added to iAS cells from *APOE3* and *APOE4* genotypes for 3 days. Afterwards, exosomes were isolated from conditioned media and characterized using NTA. The mean and median sizes of exosomes isolated from all conditions fell below 200 nm in diameter, typical of exosome range (**Figure 6A**). The quantity of exosomes secreted per cell showed a significant difference between *APOE3* and *APOE4* iAS cells, both naïve and when treated with oleic acid. Additionally, exosome secretion per cell increased whenever cells were treated with oleic acid (**Figure 6B**). When exosome yield is normalized to media consumption, the same trends are observed (**Figure 6C**). Overall, these results suggest that under lipid stress, exosome secretion is increased in both *APOE* genotypes, though *APOE3* cells secrete a significantly larger number of exosomes than *APOE4* cells, suggesting dysregulation of ESCRT activity in *APOE4* astrocytes.

Using the THP-1 cells, modulations in the inflammatory capacity of astrocyte exosomes due to lipid stress were evaluated. As before, the addition of exosomes from DMSO vehicle-treated *APOE4* iAS cells induced a significant increase in NF-κB activity, a trait not seen in *APOE3* iAS exosomes. An increase in inflammatory activation was also seen when comparing exosomes from oleic acid treated- *APOE4* iAS cells to unstimulated controls. However, no difference between unstimulated control and THP-1 cells treated with oleic acid stimulated *APOE3* iAS exosomes was observed (**Figure 6D**). Overall, this suggests that while oleic acid can alter the

exosome secretion of cells from *APOE3* and *APOE4* genotypes, only those from *APOE4* backgrounds mediate inflammatory signaling under lipid stress.

3.5. *APOE* Genotype Alters EV Lipid Composition Based on Quantitative Lipidomics

Due to the role both APOE and exosomes play in facilitating lipid transport, understanding changes in exosome lipid composition in APOE4 is important. To do so, lipidomic analysis was performed, comparing the lipid profile of exosomes derived from *APOE3* and *APOE4* astrocytes. PCR analysis showed that the lipid profiles of exosomes derived from the two genotypes form distinct clusters (**Figure 7A**). It was discovered that APOE4 derived exosomes had higher total lipid content compared to APOE3 derived exosomes (**Figure 7B**). Lipids from different classes were identified and sorted to give their yield based upon class. From this, it was revealed that APOE4 derived exosomes display higher levels of cholesterol, biliary acids, and sphingolipids, while also showing lower levels of sphingomyelin (**Figure 7C, 7D, 7E, 7F**). Lysophospholipid levels also showed a general upregulation within APOE4 derived exosomes, especially in lysophosphatidic acid (LPA) and lysophosphatidylcholines (LPC) (**Figure 7G**). In the context of AD, LPC typically display neuroprotective properties, excluding those with 16 and 18 carbon fatty acid chains which are associated with Alzheimer's Disease progression. Therefore, the carbon chain length of LPCs was investigated, revealing that 16 and 18 carbon chain length carbons are upregulated in APOE4 exosome LPCs. LPAs, a metabolic product of LPCs, also displayed this trend (**Figure 7H**).

A full breakdown of each lipid species detected and differentially regulated was performed. A volcano plot reveals a total of 121 differentially expressed lipid species: 88 upregulated in APOE4 and 33 downregulated (**Figure 8A**). Heatmap analysis and scatter plotting showed that of the species upregulated, several belonged to the lipid families of biliary acids, lysophospholipids, sphingolipids, and carnitines (**Figure 8B,8C**). From the differentially expressed lipids, the top 20 were identified based upon fold change. Of the identified differentially expressed lipids, 19 were upregulated in APOE4 derived exosomes, including LPS18:0, lysophosphatidylinositol (LPI) 18:0, and lysophosphatidylglycerol (LPG) 18:0 (**Figure 8D**). Accompanying this, KEGG analysis was performed on differentially expressed lipids to identify lipid metabolic pathways altered in APOE4 astrocyte exosomes. From KEGG analysis, the top differentially expressed pathways include efferocytosis, glycerophospholid metabolism, primary bile acid synthesis, and choline metabolism in cancer **(Figure 8E, Supplementary Figure S1, S2, S3, S4**). Overall, lipidomic analysis of APOE3 and APOE4 astrocyte-derived exosomes

reveals that exosomes of APOE4 lead to the dysregulation of several lipids involved in AD progression and diagnosis.

4. Discussions

APOE4 is the strongest single genetic predictor of AD development, disrupting neural metabolic processes. The single amino-acid substitution in the *APOE4* genotype disrupts the lipid binding domain of the lipoprotein, leading to a loss in ability to bind free cholesterol and regulate its transport. Exosomes, membrane-bound mediators of paracrine transport, have been shown to carry APOE particles, aiding in the progression of APOE4-related AD. In this study, we sought to evaluate the extent to which APOE3 and APOE4 affect the biogenesis and biological properties of exosomes and the role they play in AD progression.

Quantification of exosome release revealed a significant decrease in biogenesis in astrocytes derived from the *APOE4* genotype. This is associated with downregulation of exosome biogenesis gene expression for both ESCRT dependent and independent pathways. Previous research has shown that endosomal formation is one of the first signs of AD development [35, 36]. Since exosome biogenesis is dependent upon the endosomal compartment, it is likely that this disruption is partially responsible for the decrease in exosome release seen in APOE4 cells [37, 38]. Furthermore, lipid profiling revealed a dysregulation of lipids involved in exosome biogenesis, namely sphingomyelin. Sphingomyelin is metabolized by SMase proteins into ceramide to facilitate the inward budding of multivesicular bodies to form intraluminal vesicles, precursors to exosomes [39-41]. Here we reported lower levels of sphingomyelin in *APOE4* astrocyte-derived exosomes without a correlated increase in ceramide levels suggest dysregulated sphingomyelin levels inhibit intraluminal vesicle formation. However, further study on endosomal sorting and multivesicular body formation with *APOE4* is needed to draw conclusions.

Inhibition of APOE4 exosome biogenesis was accompanied by an increase of exosome-mediated proinflammatory signaling observed in THP-1 assays. Results showed an increase in NF-κB signaling after treatment with APOE4 exosomes derived from astrocytes and mesenchymal stromal cells, including exosomes derived from astrocytes in a model of lipid stress. While the exact mechanism by which inflammation was induced is not certain, some hypotheses can be put forth based upon lipidomic analysis. The total lipid content observed in APOE4 astrocyte-derived exosomes compared to their APOE3 counterparts suggests that excess lipid

accumulation is a possible mechanism for inducing inflammation, consistent with previous findings in Alzheimer's Disease research [42-44]. Additionally, upregulated levels of cholesterol and lysophospholipids were observed in APOE4 exosomes. Cholesterol serves as a major lipid class accumulated in neural tissue in Alzheimer's disease progression and has previously been linked to neuroinflammation as the disease progresses [45-47]. Lysophospholids, products of the breakdown of phospholipids, play a mixed role in Alzheimer's progression and inflammation. But certain classes of lysophospholids, such as lysophosphatidyl serine, are pro-inflammatory and significantly upregulated in APOE4 exosomes [48, 49]. The multitude of potential inflammatory etiologies makes coming to conclusions difficult, with further research required to delineate cause.

In addition to previously mentioned dysregulation and the roles they play in the biogenesis and inflammatory properties of APOE4 astrocyte-derived exosomes, quantitative lipidomic analysis revealed other insights into the effects APOE4has on exosomes (**Supplementary Figure S3, S4, S5, and S6**). KEGG analysis revealed significant alteration of lipid levels in efferocytosis, choline metabolism in cancer, and bile acid synthesis. Lipid activators of efferocytosis, the programmed phagocytosis of dying cells, were upregulated in APOE4 derived exosomes, specifically lysophosphatidyl cholines and phosphatidylserines, which serve as signaling molecules for initiating recruitment and phagocytosis (**Supplementary Figure S3**) [50-52]. In Alzheimer's Disease, efferocytosis has been proposed as a potential mechanism of reducing neuroinflammation and clearing amyloid plaques [53, 54]. However, in the sole presence of efferocytosis initiating lipids suggests that APOE4 exosomes carry markers of impending apoptosis and any indication that said exosomes significantly alter immune cell activation towards efferocytosis instead of a proinflammatory polarization remains to be seen.

Bile acid synthesis represents a major pathway by which cholesterol is processed. Given the key role cholesterol plays in AD lipid stress, its conversion to a more benign form holds promise in improving disease progression. However, the products of bile acid synthesis can be either neuroprotective or further disease progression. In general, conjugated primary bile acids (CPBAs), which include cholic acid or chenodeoxycholic acid joined with taurine or glycine, are associated with the progression of AD [59-61]. Correspondingly, we observed an increase in the amount of CPBAs in *APOE4* astrocyte exosomes, specifically taurocholic acid (TCA) and taurochenodeoxycholic acid (TDCA). Glycochenodeoxycholic acid (GCDA) was detected in levels comparable to those found in *APOE3* astrocyte exosomes, while all other CPBAs were not detected in either sample (**Supplementary Figure S3**). TCA and TDCA have roles in AD that are not well-defined, though some recent studies have suggested they play minor roles promoting

AD-related symptoms [62-64]. Of note, Tauroursodeoxycholic acid (TUDCA), a metabolic product of TDCA, has been heavily investigated as a therapeutic option for AD, as it attenuates amyloid-mediated neurotoxicity, metabolic dysregulation, and combats cognitive decline [65-67]. It is possible that harnessing enzymatic conversion of TDCA to TUDCA via exogenous delivery or gene editing can prove therapeutic in Alzheimer's models, using exosomes to transfer TUDCA.

Choline metabolism plays a complex role in Alzheimer's Disease. While moderate levels of choline can help attenuate excessive neuron firing in dementia, the breakdown of choline-containing lipids such as phosphatidylcholine (PC) help drive Alzheimer's related neuron loss, as it is a major component of neural cell membranes [55, 56]. It is likely that this loss of membrane integrity is reflected in the higher content of glycerophosphatidylcholine, a metabolic product of PC breakdown, being included in exosomes (**Supplementary Figure S6**) [57, 58]. The full effect that this integrity loss has on exosome stability is unexplored but may have some relevance in disrupted exosome-mediated signaling.

5. Conclusions

To conclude, this study evaluated the effects that APOE4has upon astrocyte-derived exosomes. Results suggested that exosome biogenesis is inhibited with APOE4 due to dysregulation in both ESCRT dependent and independent pathways. They also suggested that the inflammatory properties of exosomes are modulated due to APOE4. Lipidomic analysis revealed differential lipid expression in *APOE* genotypes that relate to the observed changes in in exosome biogenesis and inflammation, namely lower levels of sphingomyelin and higher total lipid, cholesterol, and lysophospholipid levels. Upregulation of lipids in conjugated primary bile acids, choline containing lipids, and lipid signalers in efferocytosis we also observed. Overall, this suggests that exosome signaling and its dysregulation is an important mediator of AD.

6. Acknowledgements

The authors would like to thank Dr. Brian K. Washburn and Diego Zorio at FSU Department of Biological Sciences for their help with RT-qPCR analysis. The Hitachi HT7800 for TEM was funded from NSF grant 2017869. Research reported in this publication was supported by the National Science Foundation (USA) (CMMI 2100987), NSF INTERN award, and in part supported by the National Institutes of Health (USA) under Award Number R01AG090809 and R21EB033495. The content is solely the responsibility of the authors and does not necessarily represent the official views of the National Institutes of Health.

Declaration:

The authors declare that they have not used AI-generated work in this manuscript.

Ethics approval and consent to participate

Human cells (iPSCs) were purchased from the Jackson Labs. There was initial ethical approval for collection of human cells, and that the donors had signed informed consent.

Competing interests:

Authors declare that they have no competing interests.

Data and materials availability:

The datasets generated during and/or analyzed during the current study are available from the corresponding authors on reasonable request.

References

[1] K. Blennow, M.J. de Leon, H. Zetterberg, Alzheimer's disease, Lancet 368(9533) (2006) 387-403.
[2] N. Koutsodendris, M.R. Nelson, A. Rao, Y. Huang, Apolipoprotein E and Alzheimer's Disease: Findings, Hypotheses, and Potential Mechanisms, Annu Rev Pathol 17 (2022) 73-99.
[3] H.N. Yassine, C. Hugo, B. O'Donovan, I.O. Stephens, L.A. Johnson, G. Cole, J. Tcw, J. Johansson, K. Kisler, O. Chiba-Falek, APOE-Targeted Therapeutics for Alzheimer's Disease, J Neurosci 45(46) (2025).
[4] G. Bu, Apolipoprotein E and its receptors in Alzheimer's disease: pathways, pathogenesis and therapy, Nat Rev Neurosci 10(5) (2009) 333-44.
[5] R.W. Mahley, Apolipoprotein E: Cholesterol Transport Protein with Expanding Role in Cell Biology, Science 240(4852) (1988) 622-630.
[6] T. Kanekiyo, H. Xu, G. Bu, ApoE and Abeta in Alzheimer's disease: accidental encounters or partners?, Neuron 81(4) (2014) 740-54.
[7] R.W. Mahley, K.H. Weisgraber, Y. Huang, Apolipoprotein E: structure determines function, from atherosclerosis to Alzheimer's disease to AIDS, Journal of Lipid Research 50 (2009) S183-S188.
[8] Y. Huang, R.W. Mahley, Apolipoprotein E: structure and function in lipid metabolism, neurobiology, and Alzheimer's diseases, Neurobiol Dis 72 Pt A (2014) 3-12.
[9] N.E. Miller, HDL metabolism and its role in lipid transport, (0195-668X (Print)).
[10] G. Schmitz, M. Grandl, The molecular mechanisms of HDL and associated vesicular trafficking mechanisms to mediate cellular lipid homeostasis, Arterioscler Thromb Vasc Biol 29(11) (2009) 1718-22.

[11] C. Borras, A. Mercer, S. Sirisi, D. Alcolea, J.C. Escola-Gil, F. Blanco-Vaca, M. Tondo, HDL-like-Mediated Cell Cholesterol Trafficking in the Central Nervous System and Alzheimer's Disease Pathogenesis, Int J Mol Sci 23(16) (2022).
[12] P. Zhu, L. Xiao, Y. Wang, Mechanisms of high-density lipoprotein in regulating blood-brain barrier function: insights and implications, Fluids Barriers CNS 22(1) (2025) 113.
[13] S. Parhizkar, D.M. Holtzman, APOE mediated neuroinflammation and neurodegeneration in Alzheimer's disease, (1096-3618 (Electronic)).
[14] D. Dias, C.C. Portugal, J. Relvas, R. Socodato, From Genetics to Neuroinflammation: The Impact of ApoE4 on Microglial Function in Alzheimer's Disease, Cells 14(4) (2025) 243.
[15] C.-C. Liu, N. Zhao, Y. Fu, N. Wang, C. Linares, C.-W. Tsai, G. Bu, ApoE4 Accelerates Early Seeding of Amyloid Pathology, Neuron 96(5) (2017) 1024-1032.e3.
[16] S. Kaji, S.A. Berghoff, L. Spieth, L. Schlaphoff, A.O. Sasmita, S. Vitale, L. Büschgens, S. Kedia, M. Zirngibl, T. Nazarenko, A. Damkou, L. Hosang, C. Depp, F. Kamp, P. Scholz, D. Ewers, M. Giera, T. Ischebeck, W. Wurst, B. Wefers, M. Schifferer, M. Willem, K.-A. Nave, C. Haass, T. Arzberger, S. Jäkel, O. Wirths, G. Saher, M. Simons, Apolipoprotein E aggregation in microglia initiates Alzheimer's disease pathology by seeding β-amyloidosis, Immunity 57(11) (2024) 2651-2668.e12.
[17] Z. Xia, E.E. Prescott, A. Urbanek, H.E. Wareing, M.C. King, A. Olerinyova, H. Dakin, T. Leah, K.A. Barnes, M.M. Matuszyk, E. Dimou, E. Hidari, Y.P. Zhang, J.Y.L. Lam, J.S.H. Danial, M.R. Strickland, H. Jiang, P. Thornton, D.C. Crowther, S. Ohtonen, M. Gómez-Budia, S.M. Bell, L. Ferraiuolo, H. Mortiboys, A. Higginbottom, S.B. Wharton, D.M. Holtzman, T. Malm, R.T. Ranasinghe, D. Klenerman, S. De, Co-aggregation with Apolipoprotein E modulates the function of Amyloid-β in Alzheimer's disease, Nature Communications 15(1) (2024).
[18] S.-I. Lee, W. Jeong, H. Lim, S. Cho, H. Lee, Y. Jang, J. Cho, S. Bae, Y.-T. Lin, L.-H. Tsai, D.W. Moon, J. Seo, APOE4-carrying human astrocytes oversupply cholesterol to promote neuronal lipid raft expansion and Aβ generation, Stem Cell Reports 16(9) (2021) 2128-2137.
[19] G. Sienski, P. Narayan, J.M. Bonner, N. Kory, S. Boland, A.A. Arczewska, W.T. Ralvenius, L. Akay, E. Lockshin, L. He, B. Milo, A. Graziosi, V. Baru, C.A. Lewis, M. Kellis, D.M. Sabatini, L.H. Tsai, S. Lindquist, APOE4 disrupts intracellular lipid homeostasis in human iPSC-derived glia, Sci Transl Med 13(583) (2021).
[20] X. Li, J. Zhang, D. Li, C. He, K. He, T. Xue, L. Wan, C. Zhang, Q. Liu, Astrocytic ApoE reprograms neuronal cholesterol metabolism and histone-acetylation-mediated memory, Neuron 109(6) (2021) 957-970.e8.
[21] T.J. Nelson, A. Sen, Apolipoprotein E particle size is increased in Alzheimer's disease, Alzheimer's & Dementia: Diagnosis, Assessment & Disease Monitoring 11(1) (2019) 10-18.
[22] L.G. Yang, Z.M. March, R.A. Stephenson, P.S. Narayan, Apolipoprotein E in lipid metabolism and neurodegenerative disease, Trends in Endocrinology & Metabolism 34(8) (2023) 430-445.
[23] A.A. Belaidi, A.I. Bush, S. Ayton, Apolipoprotein E in Alzheimer's disease: molecular insights and therapeutic opportunities, Mol Neurodegener 20(1) (2025) 47.
[24] E. Nikitidou, P.E. Khoonsari, G. Shevchenko, M. Ingelsson, K. Kultima, A. Erlandsson, Increased Release of Apolipoprotein E in Extracellular Vesicles Following Amyloid-β

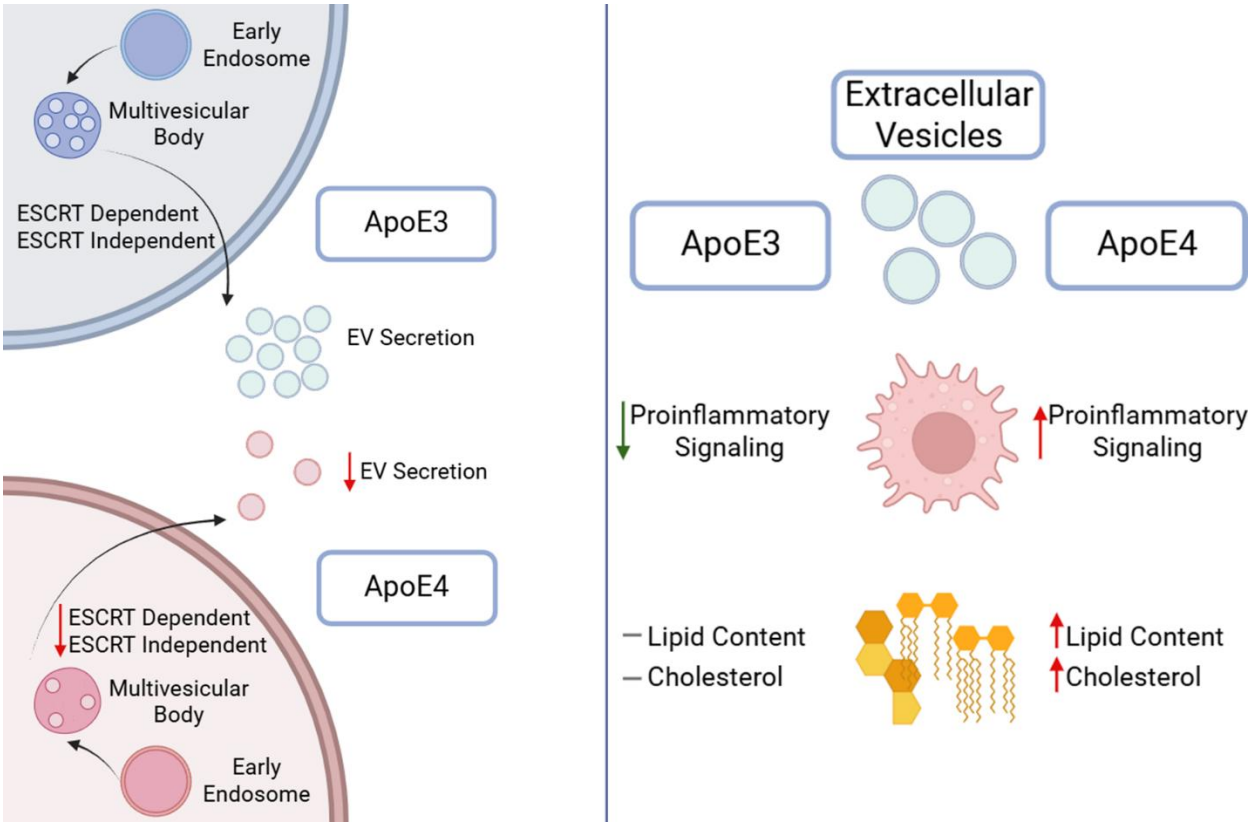
Protofibril Exposure of Neuroglial Co-Cultures, Journal of Alzheimer's Disease 60(1) (2017) 305-321.
[25] Y. Jin, Y.W. Chung, M.K. Jung, J.H. Lee, K.Y. Ko, J.K. Jang, M. Ham, H. Kang, C.G. Pack, H. Mihara, I.Y. Kim, Apolipoprotein E-mediated regulation of selenoprotein P transportation via exosomes, Cellular and Molecular Life Sciences 77(12) (2020) 2367-2386.
[26] W. Wang, N. Zhu, T. Yan, Y.-N. Shi, J. Chen, C.-J. Zhang, X.-J. Xie, D.-F. Liao, L. Qin, The crosstalk: exosomes and lipid metabolism, Cell Communication and Signaling 18(1) (2020).
[27] M. Record, K. Carayon, M. Poirot, S. Silvente-Poirot, Exosomes as new vesicular lipid transporters involved in cell–cell communication and various pathophysiologies, Biochimica et Biophysica Acta (BBA) - Molecular and Cell Biology of Lipids 1841(1) (2014) 108-120.
[28] T. Liang, Z. Wu, J. Li, S. Wu, W. Shi, L. Wang, The emerging double-edged sword role of exosomes in Alzheimer's disease, Front Aging Neurosci 15 (2023) 1209115.
[29] M. Shahlaei, H. Afkhami, A. Ahmadieh-Yazdi, S.H. Mirmazloumi, S.S. Sahraei, M. Akbari, P. Yang, H. Manoochehri, H. Tanzadehpanah, H. Mahaki, A. Sundararaman, S. Mohan, M. Sheykhhasan, S. Al-Musawi, P. Dama, Exosomes in Alzheimer's disease: From pathogenesis to therapeutics-A comprehensive review of diagnostic and drug delivery applications, Biomed Pharmacother 192 (2025) 118548.
[30] A.C. Raulin, S.V. Doss, M.G. Heckman, E.C. Craver, Z. Li, T.C. Ikezu, H. Sekiya, C.C. Liu, Y.A. Martens, C.L. Rosenberg, L.A. Kuchenbecker, M. DeTure, R.R. Reichard, A.T. Nguyen, E. Constantopoulos, R.A. Larsen, E.K. Kounaves, M.E. Murray, D.W. Dickson, R.C. Petersen, G. Bu, T. Kanekiyo, Impact of APOE on amyloid and tau accumulation in argyrophilic grain disease and Alzheimer's disease, Acta Neuropathol Commun 12(1) (2024) 25.
[31] C. Liu, L. Sun, H. Worden, J. Ene, O.Z. Zeng, J. Bhagu, S.C. Grant, X. Bao, S. Jung, Y. Li, Profiling biomanufactured extracellular vesicles of human forebrain spheroids in a Vertical Wheel bioreactor, Journal of Extracellular Biology 3 (2024) e70002.
[32] L. Muok, L. Sun, C. Esmonde, H. Worden, C. Vied, L. Duke, S. Ma, O.Z. Zeng, T.P. Driscoll, S. Jung, Y. Li, Extracellular Vesicle Biogenesis of Three-dimensional Human Pluripotent Stem Cells in a Novel Vertical-Wheel Bioreactor, Journal of Extracellular Biology 3 (2024) e133.
[33] X. Yuan, L. Sun, R. Jeske, D. Nkosi, S. York, Y. Liu, S.C. Grant, D.G.J. Meckes, Y. Li, Engineering Extracellular Vesicles by Three-dimensional Dynamic Culture of Human Mesenchymal Stem Cells, Journal of Extracellular Vesicles 11(6) (2022) e12235.
[34] R. Jeske, C. Liu, L. Duke, M.L. Canonicco Castro, L. Muok, P. Arthur, M. Singh, L. Sung, L. Sun, Y. Li, Upscaling Human Mesenchymal Stem Cell Production in a Novel Vertical Wheel Bioreactor Enhances Extracellular Vesicle Secretion and Cargo Profile, Bioactive Materials 25 (2023) 732-747.
[35] E. Nyberg, S.C. Konings, N. Lindblom, B. Israelsson, O. Klementieva, I. Martinsson, G.K. Gouras, Neuronal endolysosomal alterations induced by Apolipoprotein E4 emerge over time in primary neurons, J Biol Chem 301(8) (2025) 110479.
[36] T. Nuriel, K.Y. Peng, A. Ashok, A.A. Dillman, H.Y. Figueroa, J. Apuzzo, J. Ambat, E. Levy, M.R. Cookson, P.M. Mathews, K.E. Duff, The Endosomal-Lysosomal Pathway Is Dysregulated by APOE4 Expression in Vivo, Front Neurosci 11 (2017) 702.

[37] R. Kalluri, V.S. LeBleu, The biology, function, and biomedical applications of exosomes, Science 367(6478) (2020).
[38] Y.J. Lee, K.J. Shin, Y.C. Chae, Regulation of cargo selection in exosome biogenesis and its biomedical applications in cancer, Exp Mol Med 56(4) (2024) 877-889.
[39] D. Choezom, J.C. Gross, Neutral sphingomyelinase 2 controls exosome secretion by counteracting V-ATPase-mediated endosome acidification, J Cell Sci 135(5) (2022).
[40] D. Pieragostino, I. Cicalini, P. Lanuti, E. Ercolino, M. di Ioia, M. Zucchelli, R. Zappacosta, S. Miscia, M. Marchisio, P. Sacchetta, M. Onofrj, P. Del Boccio, Enhanced release of acid sphingomyelinase-enriched exosomes generates a lipidomics signature in CSF of Multiple Sclerosis patients, Sci Rep 8(1) (2018) 3071.
[41] C. Verderio, M. Gabrielli, P. Giussani, Role of sphingolipids in the biogenesis and biological activity of extracellular vesicles, J Lipid Res 59(8) (2018) 1325-1340.
[42] H. Chew, V.A. Solomon, A.N. Fonteh, Involvement of Lipids in Alzheimer's Disease Pathology and Potential Therapies, Front Physiol 11 (2020) 598.
[43] Y. Cao, L.W. Zhao, Z.X. Chen, S.H. Li, New insights in lipid metabolism: potential therapeutic targets for the treatment of Alzheimer's disease, Front Neurosci 18 (2024) 1430465.
[44] M. Cerasuolo, I. Di Meo, M.C. Auriemma, G. Paolisso, M. Papa, M.R. Rizzo, Exploring the Dynamic Changes of Brain Lipids, Lipid Rafts, and Lipid Droplets in Aging and Alzheimer's Disease, Biomolecules 14(11) (2024).
[45] L. Thirumangalakudi, A. Prakasam, R. Zhang, H. Bimonte-Nelson, K. Sambamurti, M.S. Kindy, N.R. Bhat, High cholesterol-induced neuroinflammation and amyloid precursor protein processing correlate with loss of working memory in mice, J Neurochem 106(1) (2008) 475-85.
[46] G. Di Paolo, T.W. Kim, Linking lipids to Alzheimer's disease: cholesterol and beyond, Nat Rev Neurosci 12(5) (2011) 284-96.
[47] F.M. Feringa, R. van der Kant, Cholesterol and Alzheimer’s Disease; From Risk Genes to Pathological Effects, Frontiers in Aging Neuroscience 13 (2021).
[48] M. Hachem, H. Nacir, Emerging Role of Phospholipids and Lysophospholipids for Improving Brain Docosahexaenoic Acid as Potential Preventive and Therapeutic Strategies for Neurological Diseases, Int J Mol Sci 23(7) (2022).
[49] K. Shanbhag, A. Mhetre, N. Khandelwal, S.S. Kamat, The Lysophosphatidylserines-An Emerging Class of Signalling Lysophospholipids, J Membr Biol 253(5) (2020) 381-397.
[50] R.B. Birge, S. Boeltz, S. Kumar, J. Carlson, J. Wanderley, D. Calianese, M. Barcinski, R.A. Brekken, X. Huang, J.T. Hutchins, B. Freimark, C. Empig, J. Mercer, A.J. Schroit, G. Schett, M. Herrmann, Phosphatidylserine is a global immunosuppressive signal in efferocytosis, infectious disease, and cancer, Cell Death Differ 23(6) (2016) 962-78.
[51] B. Moon, S. Yang, H. Moon, J. Lee, D. Park, After cell death: the molecular machinery of efferocytosis, Exp Mol Med 55(8) (2023) 1644-1651.
[52] R. Pandit, H. Hillman, J.W. Williams, A. Yurdagul, More Than a Cleanup Crew: The Expanding Biology of Efferocytosis, Arteriosclerosis, Thrombosis, and Vascular Biology 46(2) (2026) e323211.

[53] Y. Chen, Y. Kou, Y. Ni, H. Yang, C. Xu, H. Fan, H. Liu, Microglia efferocytosis: an emerging mechanism for the resolution of neuroinflammation in Alzheimer's disease, J Neuroinflammation 22(1) (2025) 96.
[54] S. Kanuri, Repercussions of microglial efferocytosis on neurodegeneration in Alzheimer's Disease (AD): a double-edged sword and perplexing factor warranting scrutiny in AD research, The Egyptian Journal of Neurology, Psychiatry and Neurosurgery 60(1) (2024).
[55] J.K. Blusztajn, B.E. Slack, Accelerated Breakdown of Phosphatidylcholine and Phosphatidylethanolamine Is a Predominant Brain Metabolic Defect in Alzheimer's Disease, J Alzheimers Dis 93(4) (2023) 1285-1289.
[56] L. Whiley, A. Sen, J. Heaton, P. Proitsi, D. García-Gómez, R. Leung, N. Smith, M. Thambisetty, I. Kloszewska, P. Mecocci, H. Soininen, M. Tsolaki, B. Vellas, S. Lovestone, C. Legido-Quigley, Evidence of altered phosphatidylcholine metabolism in Alzheimer's disease, Neurobiol Aging 35(2) (2014) 271-8.
[57] J.K. Blusztajn, I. Lopez Gonzalez-Coviella, M. Logue, J.H. Growdon, R.J. Wurtman, Levels of phospholipid catabolic intermediates, glycerophosphocholine and glycerophosphoethanolamine, are elevated in brains of Alzheimer's disease but not of Down's syndrome patients, Brain Res 536(1-2) (1990) 240-4.
[58] A. Walter, U. Korth, M. Hilgert, J. Hartmann, O. Weichel, M. Hilgert, K. Fassbender, A. Schmitt, J. Klein, Glycerophosphocholine is elevated in cerebrospinal fluid of Alzheimer patients, Neurobiology of Aging 25(10) (2004) 1299-1303.
[59] H.D. Ackerman, G.S. Gerhard, Bile Acids in Neurodegenerative Disorders, Front Aging Neurosci 8 (2016) 263.
[60] P. Baloni, C.C. Funk, J. Yan, J.T. Yurkovich, A. Kueider-Paisley, K. Nho, A. Heinken, W. Jia, S. Mahmoudiandehkordi, G. Louie, A.J. Saykin, M. Arnold, G. Kastenmuller, W.J. Griffiths, I. Thiele, C. Alzheimer's Disease Metabolomics, R. Kaddurah-Daouk, N.D. Price, Metabolic Network Analysis Reveals Altered Bile Acid Synthesis and Metabolism in Alzheimer's Disease, Cell Rep Med 1(8) (2020) 100138.
[61] K. Nho, A. Kueider-Paisley, S. MahmoudianDehkordi, M. Arnold, S.L. Risacher, G. Louie, C. Blach, R. Baillie, X. Han, G. Kastenmuller, W. Jia, G. Xie, S. Ahmad, T. Hankemeier, C.M. van Duijn, J.Q. Trojanowski, L.M. Shaw, M.W. Weiner, P.M. Doraiswamy, A.J. Saykin, R. Kaddurah-Daouk, I. Alzheimer's Disease Neuroimaging, C. the Alzheimer Disease Metabolomics, Altered bile acid profile in mild cognitive impairment and Alzheimer's disease: Relationship to neuroimaging and CSF biomarkers, Alzheimers Dement 15(2) (2019) 232-244.
[62] M. McMillin, G. Frampton, S. Grant, S. Khan, J. Diocares, A. Petrescu, A. Wyatt, J. Kain, B. Jefferson, S. DeMorrow, Bile Acid-Mediated Sphingosine-1-Phosphate Receptor 2 Signaling Promotes Neuroinflammation during Hepatic Encephalopathy in Mice, Front Cell Neurosci 11 (2017) 191.
[63] Z. Ren, L. Zhao, M. Zhao, T. Bao, T. Chen, A. Zhao, X. Zheng, X. Gu, T. Sun, Y. Guo, Y. Tang, G. Xie, W. Jia, Increased intestinal bile acid absorption contributes to age-related cognitive impairment, Cell Rep Med 5(5) (2024) 101543.
[64] Y. Mo, Y. Peng, I. Alzheimer's disease Neuroimaging, Bile acid profile and white matter microstructural changes in early Alzheimer's disease, Brain Res Bull 234 (2026) 111642.

[65] P.A. Dionísio, J.D. Amaral, M.F. Ribeiro, A.C. Lo, R. D'Hooge, C.M.P. Rodrigues, Amyloid-β pathology is attenuated by tauroursodeoxycholic acid treatment in APP/PS1 mice after disease onset, Neurobiology of Aging 36(1) (2015) 228-240.
[66] A.C. Lo, Z. Callaerts-Vegh, A.F. Nunes, C.M.P. Rodrigues, R. D'Hooge, Tauroursodeoxycholic acid (TUDCA) supplementation prevents cognitive impairment and amyloid deposition in APP/PS1 mice, Neurobiology of Disease 50 (2013) 21-29.
[67] R.M. Ramalho, A.F. Nunes, R.B. Dias, J.D. Amaral, A.C. Lo, R. D'Hooge, A.M. Sebastião, C.M.P. Rodrigues, Tauroursodeoxycholic acid suppresses amyloid β-induced synaptic toxicity in vitro and in APP/PS1 mice, Neurobiology of Aging 34(2) (2013) 551-561.

Graphical Abstract



List of Figures

Figure 1. Differentiation and Characterization of iPSC-derived Astrocytes (iAS). (A) Differentiation timeline for induced neural progenitor cells and induced astrocytes. (B) Immunostaining images of astrocytes derived from *APOE33* and *APOE44* iPSCs for astrocyte markers GFAP and S100β. Scale bar: 100 μm. (C) APOE4 secretion by the iAS cells from *APOE33* and *APOE44* iPSCs.

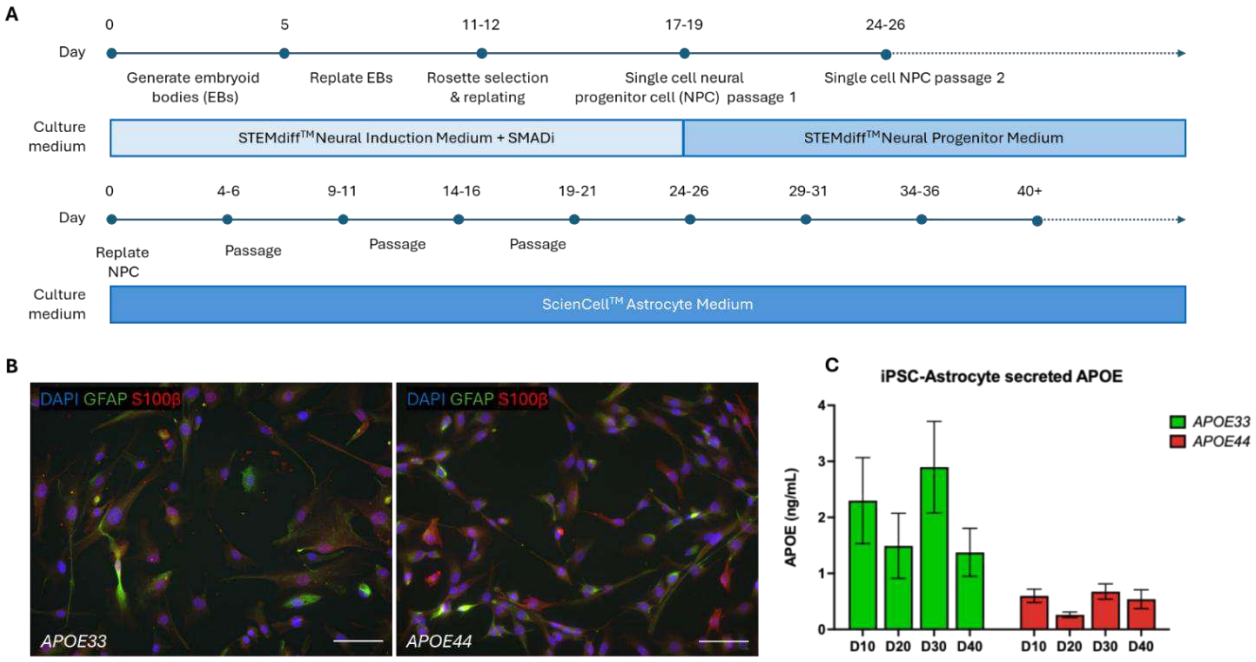


Figure 2. Differentiation and Characterization of iPSC-derived Mesenchymal Stem Cells (iMSC). (A) Differentiation timeline for iMSCs. (B,C) Flow cytometry for MSC positive markers CD73 (i), CD90 (ii), CD105 (iii), and negative marker CD44 (iv) for *APOE3* (B) and *APOE4* (C) iPSCs.

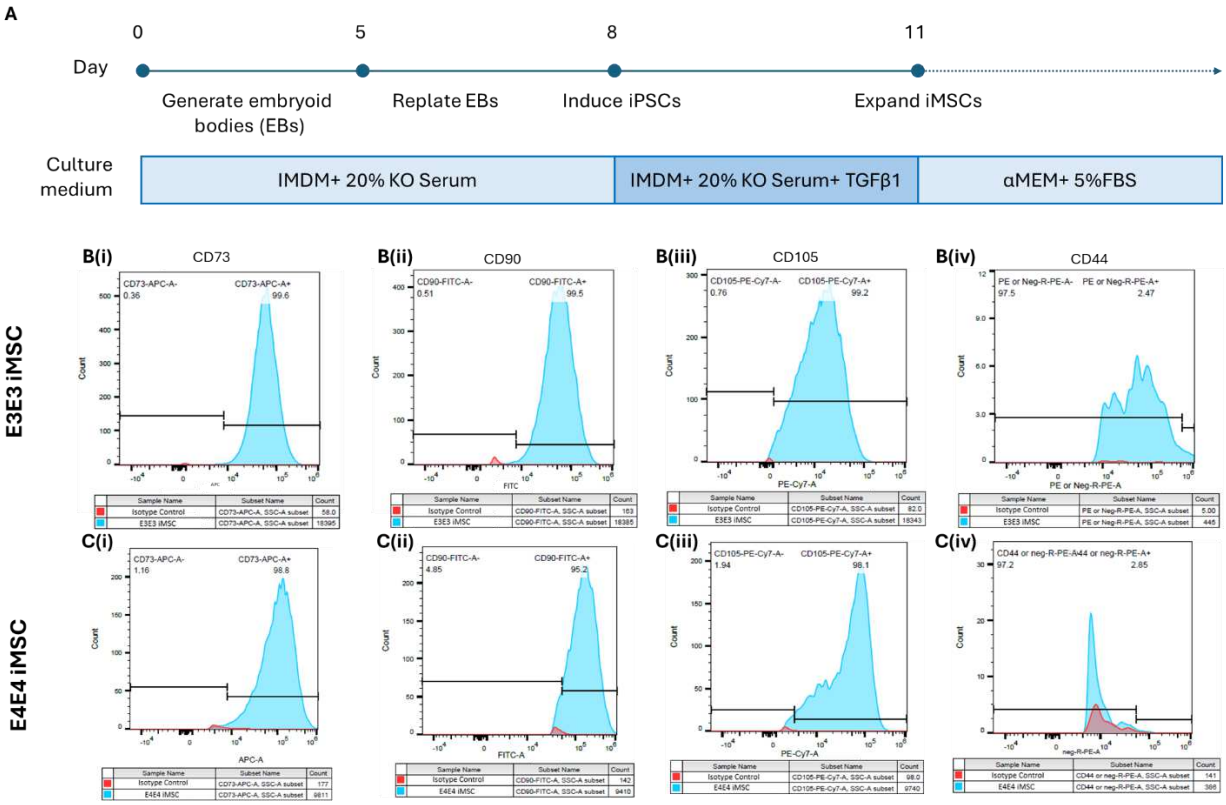


Figure 3. Characterization of iAS-derived Exosomes from APOE3 and APOE4 Genotypes. (A) NTA Size histograms of iAS-derived exosomes from (i) *APOE3* and (ii) *APOE4* cells. (B) Mean and mode exosome sizes as determined by NTA. (C) iAS exosome yield normalized to cell per day of EV collection. (D) iAS exosome yield normalized to volume of media used in EV isolation. (E) TEM images of the isolated EVs: left-E3/E3 iAS EVs; right- E4/E4 iAS EVs; (F) Western blot for EV markers; (G) EV biogenesis gene expression. N=3. * indicates p<0.05. ** indicates p<0.01. *** indicates p<0.001.

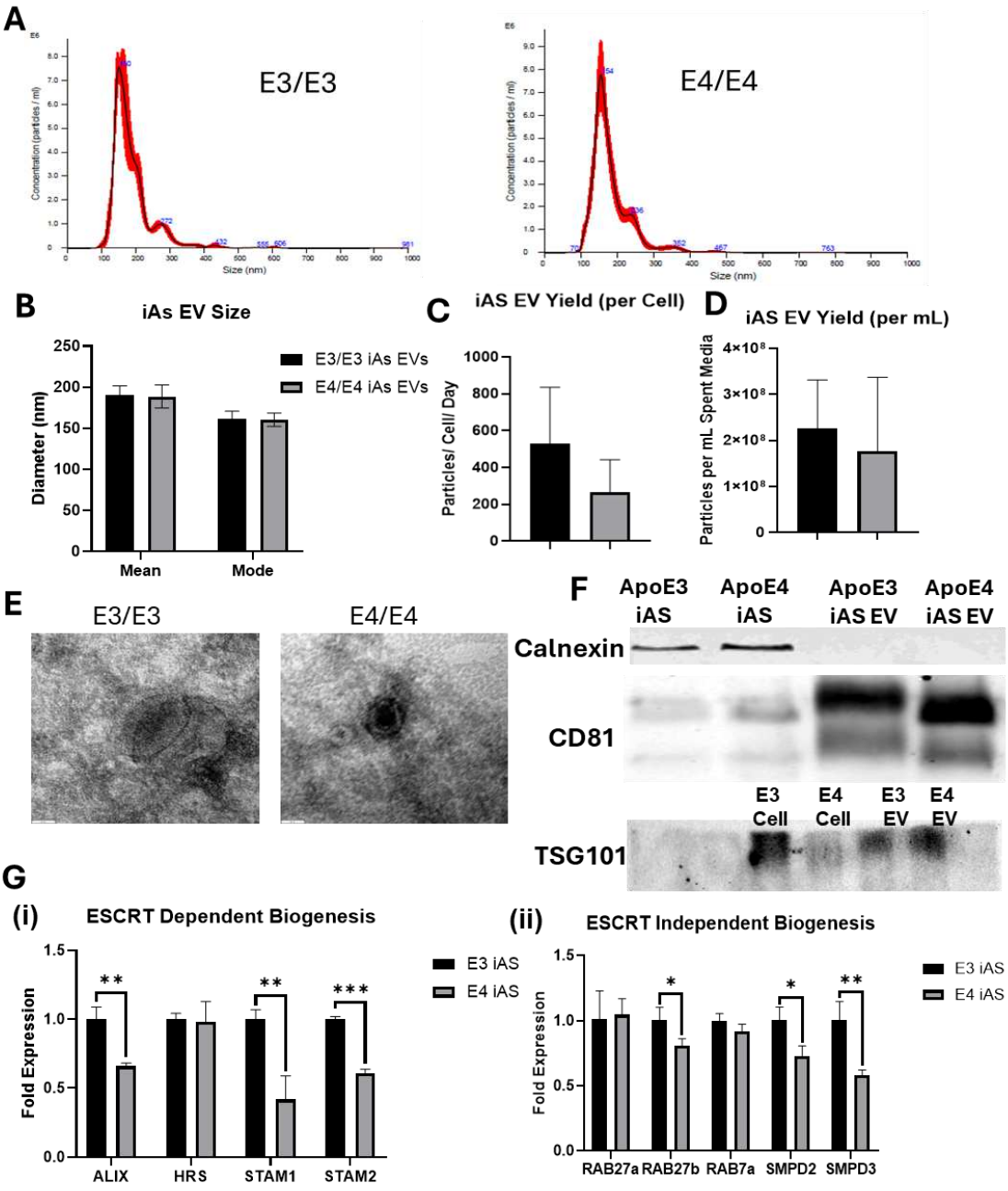


Figure 4: Characterization of iMSC-derived Exosomes from *APOE3* and *APOE4* Genotypes. (A) NTA Size histograms of iMSC- derived exosomes from (i) *APOE3* and (ii) *APOE4* cells. (B) Mean and mode exosome sizes as determined by NTA. (C) iMSC exosome yield normalized to cell per day of EV collection. (D) iMSC exosome yield normalized to volume of media used in EV isolation. (E) TEM images of the isolated EVs; left-E3/E3 iMSC EVs; right- E4/E4 iMSC EVs; (F) Western blot for EV markers. N=3. No statistical difference was observed.

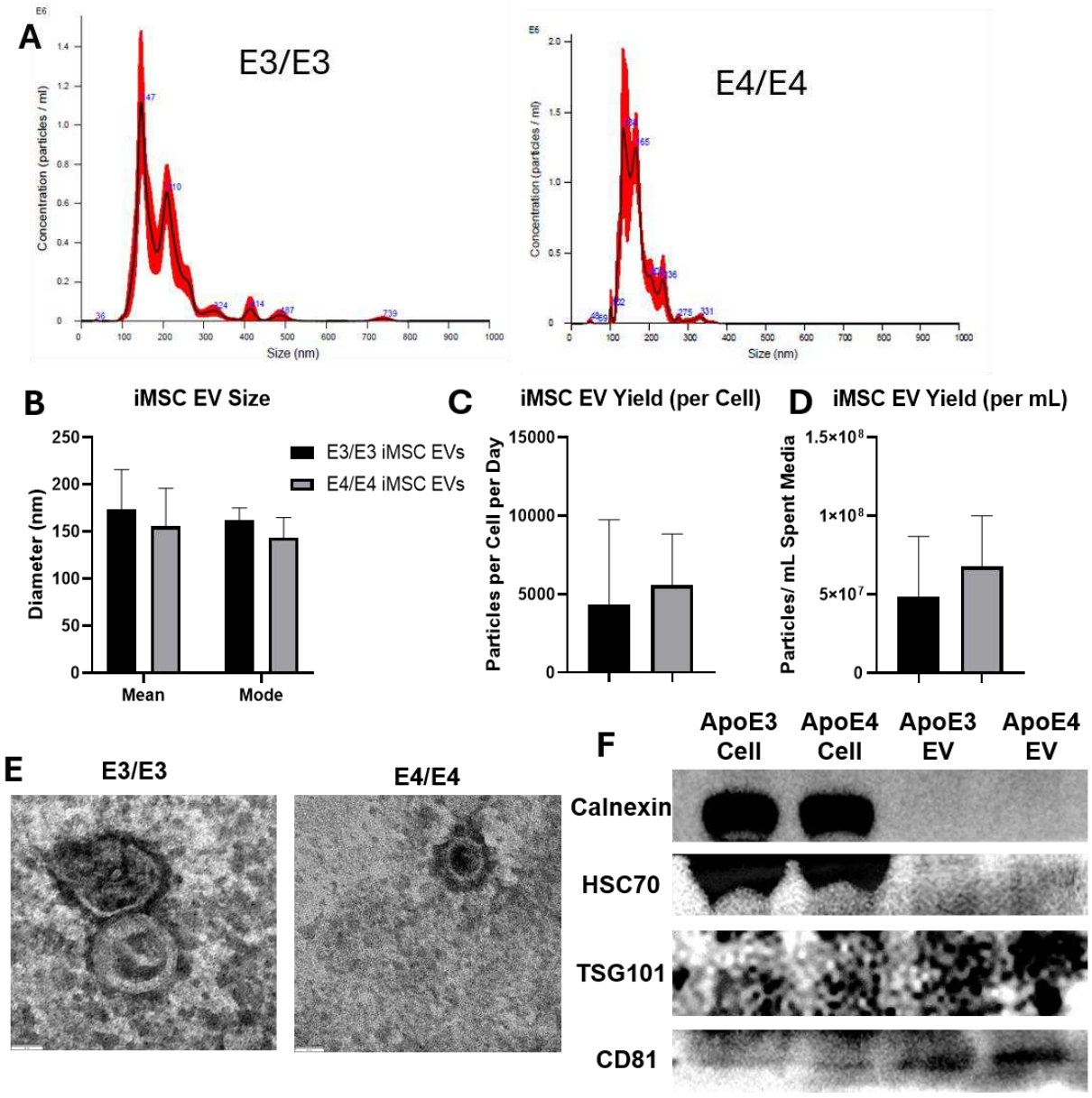


Figure 5. Inflammatory Modulation of iAS and iMSC Exosomes from Differing *APOE* Genotypes. (A) THP-1 NF-κB activation when treated with (i) low doses and (ii) high doses of iAS exosomes. (B) THP-1 NF-κB activation when treated with LPS for 6 hours before receiving (i) low doses and (ii) high doses of iAS exosomes. Inflammatory Modulation of iMSC Exosomes from Differing *APOE* Genotypes. THP-1 NF-κB activation when treated with iMSC EVs when receiving (E) no LPS pretreatment and (F) 6 hours of LPS pretreatment before exosome treatment. N=3. * indicates p<0.05.

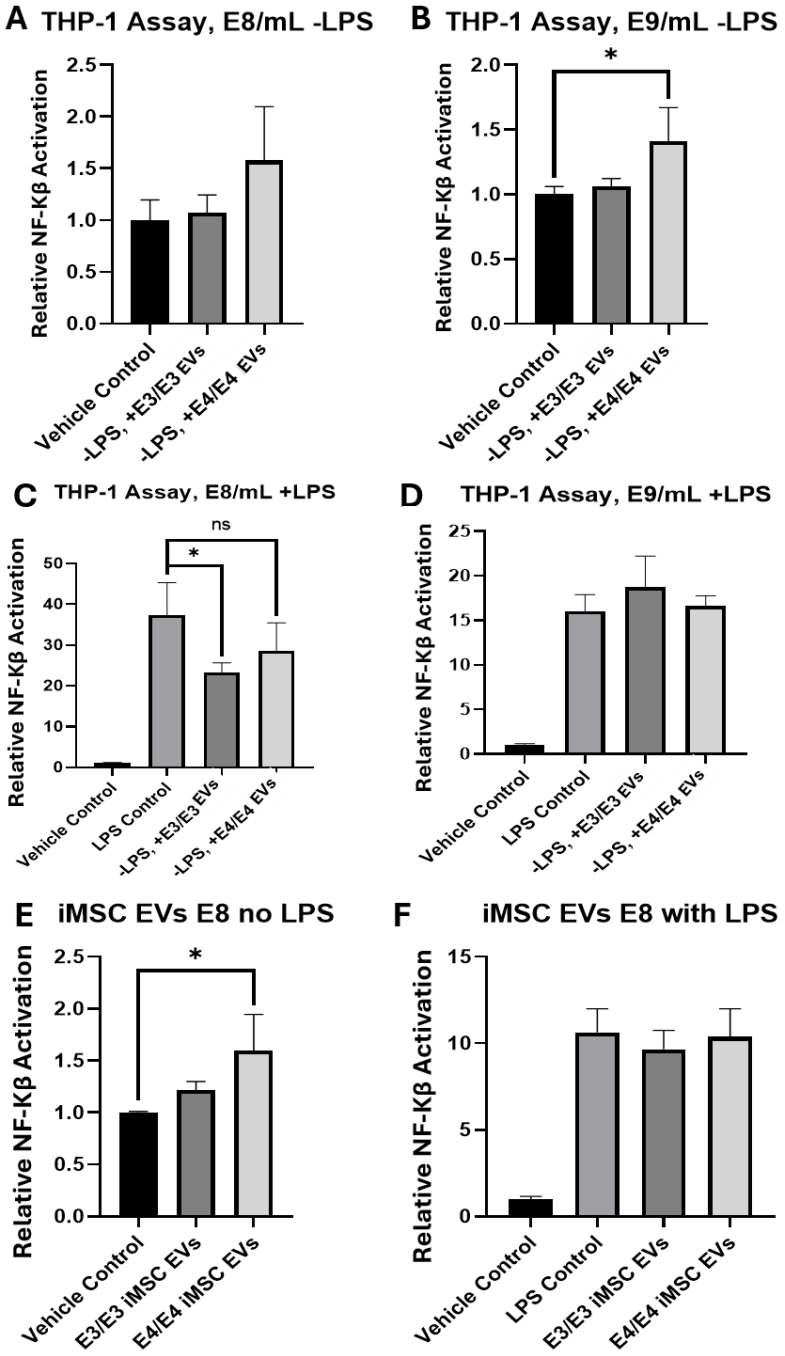


Figure 6. Lipid Stress Modulates the Secretion of Exosomes and Alters Their Inflammatory Signaling. (A) Mean and Mode sizes of iAS exosomes with APOE3 or APOE4 genotypes, either stimulated with oleic acid or receiving DMSO vehicle control. (B) Exosome yield per cell per day of exosome collection. (C) Exosome yield normalized to volume of collection media. (D) THP-1 NF-κB activation when receiving exosomes with different combinations of lipid stress and *APOE* genotype. N=3. * indicates p<0.05. ** indicates p<0.01. *** indicates p<0.001.

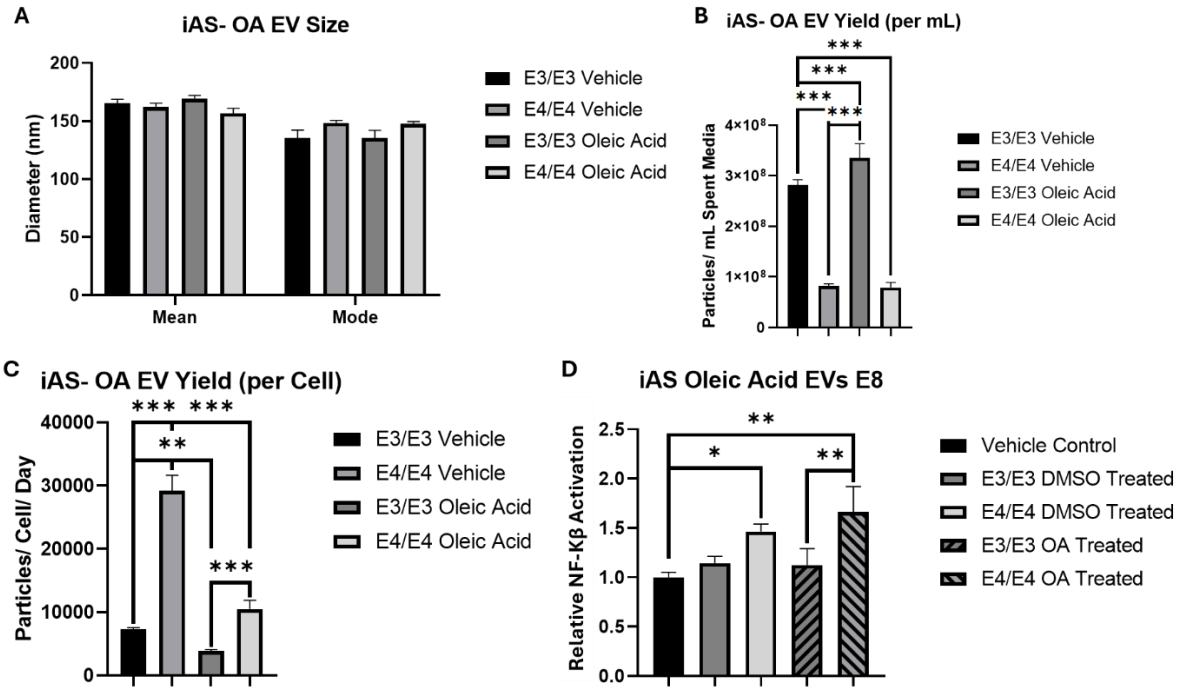


Figure 7. Lipidomics analysis of iAS-derived EVs for lipid contents. (A) PCA plot of *APOE3* and *APOE4*-astrocyte derived EV lipidomics. (B) Total lipid quantification from lipidomics. (C-G) Lipid content of lipid classes cholesterol, biliary acids, sphingolipids, sphingomyelin, and lysophospholipids. (H) Chain length of LPC (Hi) and LPA (Hii). N=3 * indicates p<0.05. ** indicates p<0.01.

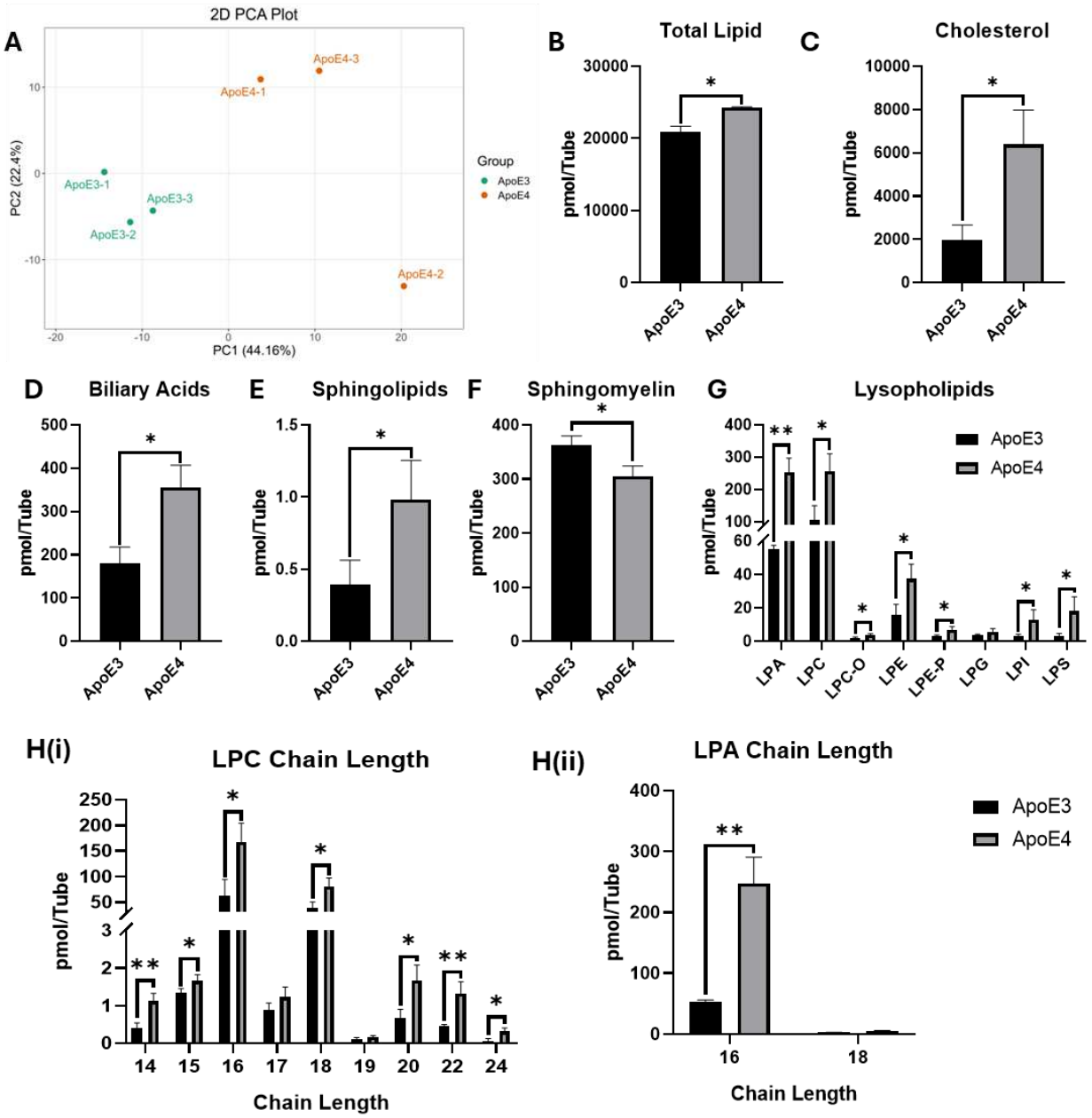
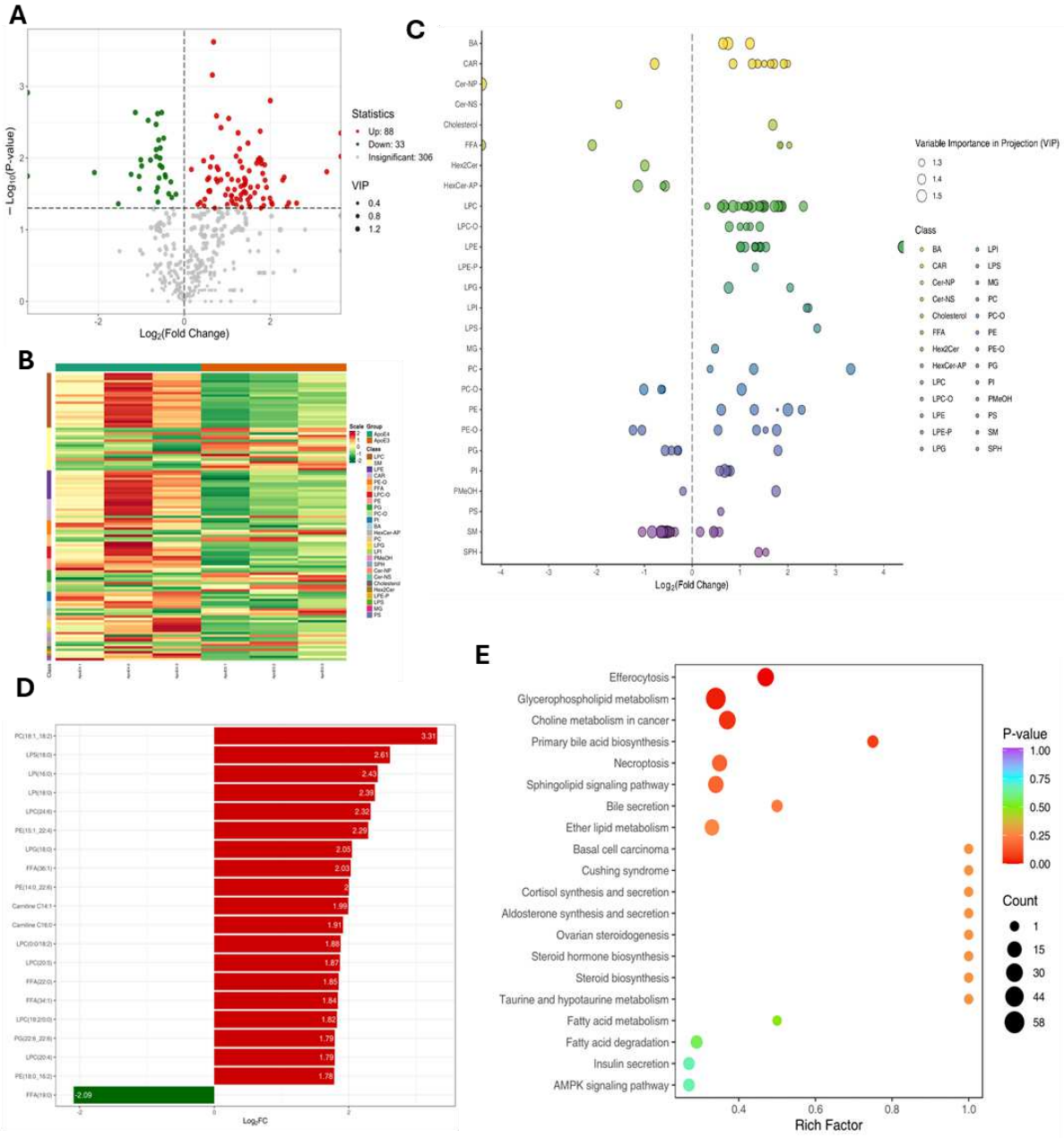


Figure 8. Lipidomics analysis of iAS-derived EVs for differential lipid expression. (A) Volcano plot of differentially expressed lipids. (B) Heatmap graph of differentially expressed lipids. (C) Scatterplot of differentially expressed lipids. (D) Top 20 differentially expressed lipids. (E) KEGG pathway analysis based on differentially expressed lipids.



Supplementary Files

This is a list of supplementary files associated with this preprint. Click to download.

- E4iASCEVADSuppleEsmonde20261008YL.docx
- SupplementaryDataFigureS1Figure1ELISA.xlsx
- SupplementaryDataFIleS2CEAPOE4.xlsx